Turkish Journal of Chemistry

http://journals.tubitak.gov.tr/chem/

Research Article

Turk J Chem
(2016) 40: 147 – 162

doi:10.3906/kim-1504-32

Adsorptive features of polyacrylamide–aluminosilicate composites for methylene blue

Demet BAYBAŞ[1,*], **Ulvi ULUSOY**[2]

[1]Department of Biochemistry, Faculty of Science, Cumhuriyet University, Sivas, Turkey
[2]Department of Chemistry, Faculty of Science, Cumhuriyet University, Sivas, Turkey

Received: 13.04.2015 • **Accepted/Published Online:** 07.08.2015 • **Final Version:** 05.01.2016

Abstract: Polyacrylamide–montmorillonite (PAAm-Mt) and polyacrylamide–clinoptilolite (PAAm-Z) composites were prepared by cross-linked polymerization of acrylamide in dispersions of Mt and Z. The composites were characterized by FT-IR, SEM, XRD, CEC, and PZC analysis. The adsorptive features of PAAm-Mt and PAAm-Z for methylene blue (MB) were investigated by their relevance to initial dye concentration, temperature, contact time, PZC, and pH. The monolayer adsorption capacities were 0.14 and 0.08 mol kg^{-1} for PAAm-Z and PAAm-Mt, respectively. The changes in pH of MB solution had an insignificant influence on their adsorption capacities. The values of enthalpy and entropy changes were positive ($\Delta H_{PAAm-Mt}$ = 7.6 and ΔH_{PAAm-Z} = 17.6 kJ mol^{-1}, $\Delta S_{PAAm-Mt}$ = 55.7, and ΔS_{PAAm-Z} = 107.2 J mol^{-1} K^{-1}). The negative free enthalpy change was proof of the spontaneity of adsorption ($\Delta G_{PAAm-Mt}$ = –9.0, ΔG_{PAAm-Z} = –14.4 kJ mol^{-1}). The adsorption kinetics obeyed a pseudo-second order model ($k_{PAAm-Mt}$ = 11.5 and k_{PAAm-Z} = 1.18 mol^{-1} kg min^{-1}, R^2 > 0.99). The adsorption mechanism was the combination of chemical and physical adsorption governed by Coulombic forces (liquid film diffusion) on which the contribution of intraparticle diffusion was not significant. This was consistent with a low value of the adsorption activation energy (E_a = 9.4 kJ mol^{-1}). The composites had amphoteric features buffering the pH of the studied adsorption environment to approximately neutral levels.

Key words: Adsorption, methylene blue, aluminosilicate, composite, polyacrylamide

1. Introduction

Dyes enter the environment via wastewater streams of the dyeing, textile, tannery, and paint industries.[1] Because the majority of dyes are synthetic, containing aromatic rings, they are potentially carcinogenic and mutagenic. The removal of dyes from the aquatic environment is troublesome, because of their inertness, nonbiodegradability, and resistance to fading by exposure to light, water, and many chemicals.[2] Therefore, when the results of studies in recent decades are taken into consideration, it is seen that there is still a need for research into the proper treatment of wastewater streams at source before discharge into the environment.[3]

Physiochemical methods such as coagulation, flocculation, ion exchange, membrane separation, photodegradation, and electrochemical oxidation have been used for the treatment of contaminated water. Among them, adsorption is the most efficient, promising, and widely used in wastewater treatment because of its simplicity, economic viability, technical feasibility, and social acceptability.[4]

*Correspondence: dbaybas@cumhuriyet.edu.tr

Methylene blue (MB) (Figure 1), which is the subject of interest in this investigation, has long been used as a model for the adsorption of organic dye from aqueous solutions.[5] It is a basic cationic dye classified under the 'thiazin dyes' (color index: CI 52015 or Basic blue 9).[6] MB is also toxic such that it might cause permanent eye injury in the event of contact with the eyes, and rapid breathing or difficulty in breathing for a short period upon its inhalation, while ingestion through the mouth might result in a burning sensation, nausea, vomiting, profuse sweating, mental confusion, and methemoglobinemia.[7]

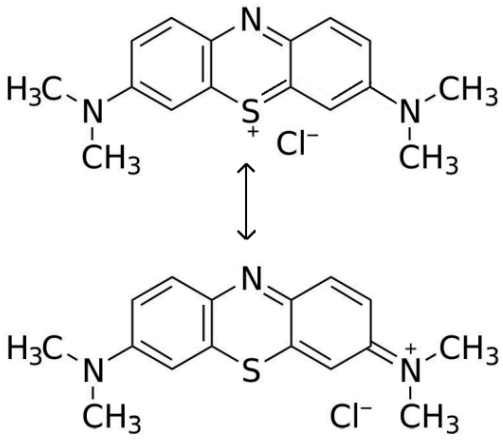

Figure 1. Molecular structure of MB.

Adsorption implementations to accomplish MB removal cover a wide variety of low cost materials. The following adsorbents exemplify the recent investigations considering beech sawdust,[1] kaolinite,[8] spinel magnesium aluminate nanoparticles,[9] modified and/or unmodified montmorillonite/clay,[10–13] sepiolite,[14] zeolite,[15–18] silica nanosheets derived from vermiculite,[19] cotton wastes,[20] biosorbents like modified *Ficus carica*,[4] polymeric sorbents such as cross-linked poly(hydroxymethylacrylamide-*co*-acrylic acid)[21] and composite materials such as starch-graft-acrylic acid/Na-MMT nanocomposite hydrogels[22] and chitosan-*g*-poly(acrylic acid)/montmorillonite nanocomposites,[23] ionic composite hydrogels based on polyacrylamide and dextran sulfate,[24] polymethacrylic acid grafted cellulose/montmorillonite composite,[25] and graphene oxide-magnetite nanocomposite.[26]

Among these, clay minerals and zeolites are particularly attractive adsorbents since they are easily available at low cost due to their high abundance in nature, in addition to their excellent mechanical and thermal resistance, and large surface area thanks to their layered and lattice structure. Although aluminosilicates are desirable materials for adsorption procedures, aggregation and coagulation in aquatic environments are undesired features limiting their practical usage. This limitation can be minimized by the use of mineral/polymer composites. The polymer should be a hydrogel capable of swelling in aquatic solutions to enable the diffusion and/or transfer of the ions towards the mineral.[27] Polyacrylamide (PAAm) with a three-dimensional network and large numbers of amide side groups can meet this criterion such that it absorbs a large amount of water and shows stimuli-responsive properties to the various external parameters, e.g., temperature, pH, and solvent composition.[28] The practicality of composites has been proved with the adsorption effects of PAAm-montmorillonite/clinoptilolite composites for metal ions[27,29–31] and for MB where sodium humate/polyacrylamide/clay,[32] humic acid immobilized-polymer/montmorillonite,[33] poly(acrylamide-co-itaconic acid)/activated charcoal,[34] N-succinyl-chitosan-g-polyacrylamide/attapulgite,[35] and polyacrylamide/

sodium alginate modified montmorillonite hybrids[36] were employed. However, dye adsorption onto the composite of montmorillonite (Mt) or clinoptilolite (Z) with polyacrylamide (PAAm) has not been considered so far.

The aim of this study was to investigate the adsorptive features of PAAm-Mt and PAAm-Z. The composites were synthesized and characterized by FT-IR, SEM, XRD, cation exchange capacity (CEC), and point of zero charge (PZC) analysis; the dependence of MB adsorption on concentration, temperature, contact time, and pH was also examined. The adsorptive features were defined with parameters derived from the compatibility of experimental data to adsorption models for isotherms, kinetics, and thermodynamics. Possible adsorption mechanisms were also proposed and interpreted by considering PZC, CEC, and pH dependence of adsorption.

2. Results and discussion

2.1. Effect of MB concentration: the isotherms

The amount of dye adsorbed on the composites (Q) was calculated by Eq. (1):

$$Q = (C_i - C_e)V/w, \tag{1}$$

where Q (mol kg^{-1}) represents the amount of MB adsorbed onto adsorbent, C_i and C_e (mol L^{-1}) represent MB concentration before and after adsorption, respectively, V (L) is MB solution volume used, and w (kg) is the mass of adsorbent.

The experimentally obtained adsorption isotherms for PAAm-Mt/Z were the distribution profiles of the concentration of the adsorbate in solution and that of adsorbent at equilibrium. For provision of the parameters specific to an adsorbate and adsorbent system, the compatibility of the experimental results to Langmuir, Freundlich, and Dubinin–Radushkevich models (Eqs. (2)–(4)) was tested:

$$\text{Langmuir } Q_e = (K_L X_L C_e)/(1 + K_L C_e) \tag{2}$$

$$\text{Freundlich } Q_e = X_F C_e^{\beta} \tag{3}$$

$$\text{Dubinin–Radushkevich } Q_e = X_{DR} e^{-K_{DR}\varepsilon^2}, \tag{4}$$

where X_L (mol kg^{-1}) is the monolayer sorption capacity and K_L (L mol^{-1}) is a constant reflecting the sorption tendency. X_F and β are the Freundlich constants and the heterogeneity factor, respectively. K_{DR} is the constant related to the mean free energy of sorption, X_{DR} (mol kg^{-1}) is the theoretical saturation capacity, and ε is the Polanyi potential

$$\varepsilon = RT \ln(1 + 1/C_e), \tag{5}$$

where R and T are the ideal gas constant (8.314 J mol^{-1} K^{-1}) and absolute temperature (K), respectively. Free energy change (E_{DR}/J mol^{-1}) required to transfer 1 mol of ion from the infinity in solution to the solid surface is calculated from Eq. (6):

$$E_{DR} = (-2K_{DR})^{-1/2}. \tag{6}$$

Figure 2 and Table 1 illustrate the compatibility of the experimentally obtained MB adsorption with PAAm-Mt or PAAm-Z, and the parameters.

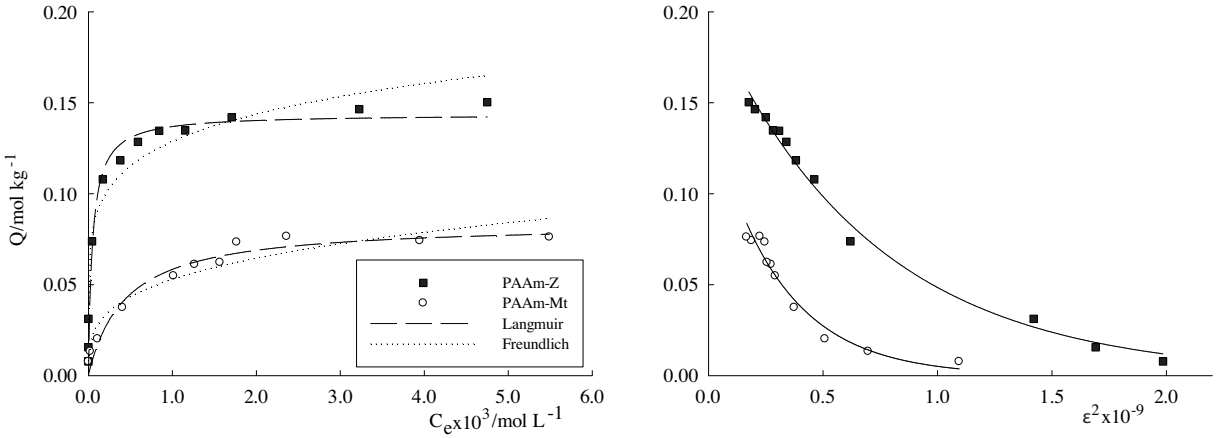

Figure 2. Experimentally obtained MB sorption onto PAAm-Z and PAAm-Mt and its compatibility to Langmuir and Freundlich (Q vs. C_e) and DR models (Q vs. ε^2).

Table 1. MB adsorption parameters derived from the Langmuir, Freundlich, and DR models.

Langmuir	PAAm-Z	PAAm-Mt
X_L (mol kg^{-1})	0.14 (0.42)*	0.08 (0.24)*
K_L (L mol^{-1})	20240	2285
R^2	0.952	0.963
Freundlich		
X_F (mol kg^{-1})	0.39	0.38
β	0.16	0.29
R^2	0.966	0.936
Dubinin–Radushkevich		
X_{DR} (mol kg^{-1})	0.20	0.15
$-K_{DR} \times 10^9$ (mol^2 K J^{-2})	1.4	3.4
R^2	0.992	0.957
E (kJ mol^{-1})	18.8	12.2

*The adsorption capacity calculated with reference to bare Mt or Z content of the composites (the mass ratio of Mt or Z to PAAm-Mt or PAAm-Z is 1/3)

The coefficients of regression obtained from the fitting of isotherms to the models of interest were statistically significant ($P < 0.05$). The isotherms were of Type-I with reference to the IUPAC physisorption classifications,[37] indicating that both composites had high affinity to MB adsorption. However, the magnitude of Langmuir monolayer adsorption capacities (X_L = 0.14 and 0.08 mol kg^{-1} for PAAm-Z and PAAm-Mt) and 'K_L' values (20240 and 2285 L mol^{-1} for PAAm-Z and PAAm-Mt, respectively) signified the adsorption tendency was in favor of PAAm-Z. The favorability was also consistent with the parameters derived from Freundlich and DR models. The adsorption parameters provided in Table 1 also referred to the 'Q' values calculated with reference to mass of the composites containing about 33% of 'Z' or 'B' in total. The preliminary investigations for adsorption of MB onto pure PAAm indicated that the adsorption capacity was not higher than 0.01 mol kg^{-1} where the initial MB concentrations were between 50 and 2000 mg L^{-1}. By neglecting the adsorption contribution of PAAm to the composites, the adsorption capacities of bare Z or Mt entrapped in the composites were expected to be three times higher than those of its composites (X_L = 0.42 and 0.24 mol

kg^{-1} for PAAm-Z and PAAm-Mt, respectively). The CEC values were 1.8 and 0.9 mol NH_4^+ kg^{-1} for Mt and PAAm-Mt, and 2.8 and 1.9 NH_4^+ kg^{-1} for Z and PAAm-Z, respectively, and were of negligible magnitude for PAAm. The calculated CECs with reference to bare Mt and Z contents of the composites (33% of composite weight) were 2.7 (0.9 × 3) and 5.7 (1.9 × 3) mol NH_4^+ kg^{-1}. Although the X_L values obtained for MB adsorption were much lower than the CEC values of composites, the composites with higher CEC also had higher X_L. The adsorption capacities lower than the expected values calculated with reference to the CECs might be attributed to the difference in molecular size and charge density (z^2/r) of NH_4^+ and MB^+, i.e. the higher adsorption capacity was in favor of NH_4^+.

The results indicate that a mineral's adsorption capacity increases because of its nano-/microscale dispersion in the polymer network (Figures 3 and 4a–4d). Moreover, when clay or clinoptilolite minerals are used in unprocessed form, they lead to aggression/coagulation problems; the practicality of the composite increases though. In fact, as seen in Table 2, both composites had considerably higher MB adsorption capacities (X_L = 157 and 89.7 mg g^{-1} for Z and Mt in PAAm-Z and PAAm-Mt, respectively, for 10 g L^{-1} adsorbent dose) than the values reported for bare minerals by taking account of the adsorbent doses (the lower dose might

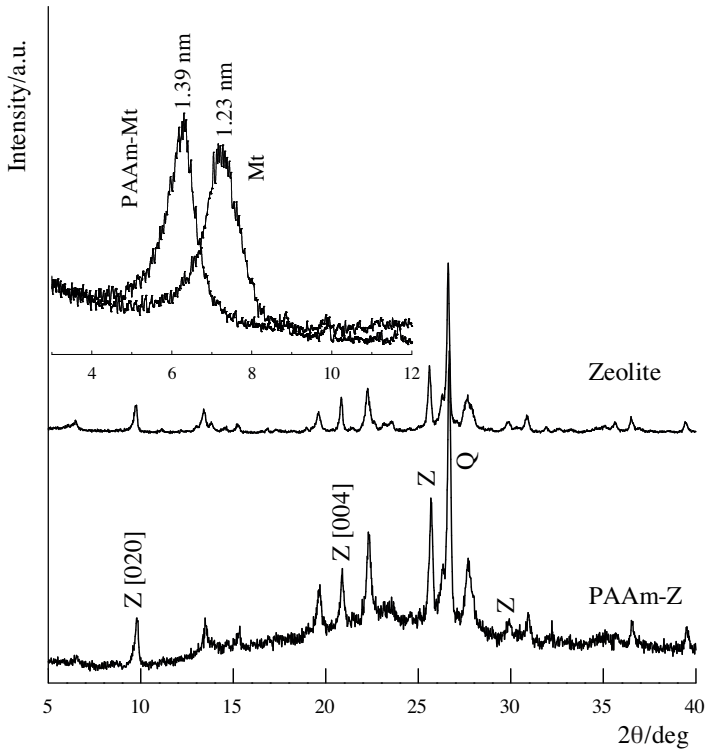

Figure 3. The characteristic d_{001} diffraction of Mt at $2\theta = 7.16^\circ$ shifted to $2\theta = 6.35^\circ$ after its conversion to PAAm-Mt. The corresponding basal spacing calculated from $d_{001} = \lambda$ / $2\mathrm{Sin}\theta$ (Bragg Low, $\lambda = 0.1542$ nm of Cu-Kα) were 1.23 and 1.39 nm. The change in basal spacing was $\Delta d_{001} = 0.20$ nm. Typical Z (Clinoptilolite) reflections (2θ = 9.75°, 22.24°, and 25.58°) also appeared in the PAAm-Z pattern without any shift (Q refers to quartz).[38] These confirmed that PAAm-Mt is an intercalated nanocomposite, 'Z' is not a layered structure mineral, and PAAm-Z is a phase-separated microcomposite.[39]

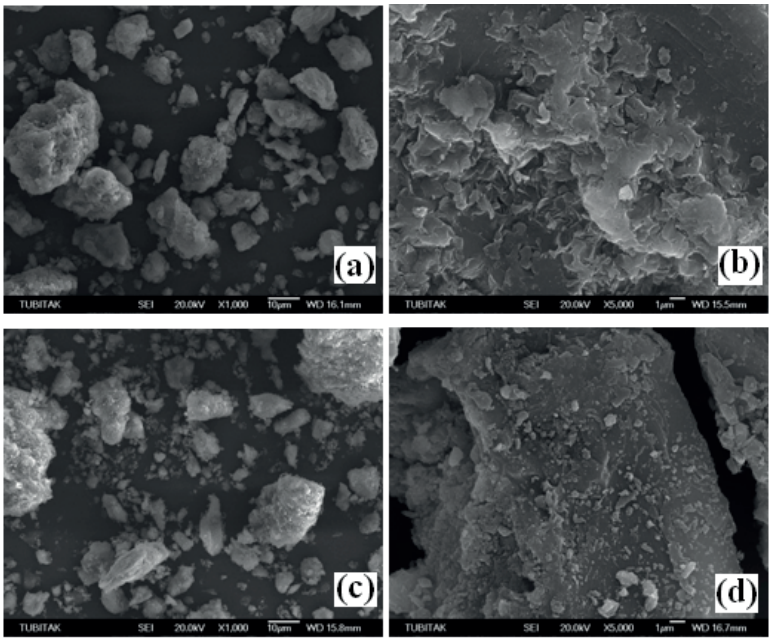

Figure 4. SEM images of Mt (a), PAAm-Mt (b), Z (c), and PAAm-Z (d) [The surface morphology of the composites had different views such that PAAm-Mt was more homogeneous than PAAm-Z due to the dissimilarities of mineralization of Mt and Z; Mt had a layered structure allowing the polymerization of acrylamide between Mt layers providing a view of material with coherent components, whilst Z had a grain structure with channel and holes with the perspective grains dispersed in PAAm].

also be the reason for higher adsorption, see Eq. (1)), e.g., 85 mg g^{-1} for Na-saturated clay minerals (5×10^{-3} g L^{-1} ads. dose),[10] 91.2 mg g^{-1} for spent clay (0.2 g L^{-1} ads. dose),[11] 58.0 mg g^{-1} for raw clay (1 g L^{-1} ads. dose),[13] and 142.2 and 222.6 mg g^{-1} for a regional montmorillonite and sepiolite, respectively (1 g L^{-1} ads. dose).[14] The capacities found in this study were also comparable with those found for the hydrogel composites provided in the Table (242.4 mg g^{-1} for HA-Am-PAAm-B for 2 g L^{-1} ads. dose and 135.1 mg g^{-1} for NSC-*g*-PAAm/APT for 4 g L^{-1} ads. dose). Consequently, the results of this study implied that PAAm-Mt and especially PAAm-Z should be considered as favorite adsorbents due to their low cost and practicality.

The dimensionless separation factor (R_L), as a measure of the adsorption favorability, was calculated (0 $< R_L <$ 1, smaller is more favorable) by using the following equation:

$$R_L = 1/(1 + K_L C_0), \tag{7}$$

where K_L the Langmuir constant,[43] ranging between 0.387 and 0.008 for PAAm-Z and 0.848 and 0.065 for PAAm-Z for initial MB concentrations in the studied ranges (25–2000 mg L^{-1}), indicating again that the adsorption was more favorable for PAAm-Z.

Further considerations of Langmuir parameters to predict the adsorbent doses (w/V as kg L^{-1}) for the removal of 50% MB from a hypothetic solution (C_0 = 100 mg L^{-1})[27] were calculated by using the following equation:

$$w/V = (C_0 - C_e)/Q = (C_0 - C_e)/[K_L X_L C_e/(1 + K_L C_e)], \tag{8}$$

Table 2. Comparison of the maximum MB adsorption capacities for different adsorbents.

Adsorbent	Dose (g L^{-1}) / pH / T(K)	X_L(mg g^{-1})	Reference
PAAm-Z	10 / 4–6 / 298	52.4 (157.2)**	This study
PAAm-Mt	10 / 4–6 / 298	29.9 (89.7) **	This study
Kaolinite	0.8 / * - / 293	7.6–20.4	[8]
Spinel magnesium aluminate nanoparticles	4 / 7 / 293	0.9	[9]
Na-saturated clay minerals	5–25 × 10^{-3} / 6.1 / 298	85–39	[10]
Spent activated clay	0.2 / 5.5 / 298	91.2	[11]
Pillared clays (Al-PILC, Zr-PILC)	10 / 7 / 298	4.1–4.3	[12]
Raw and acid/heat treated clays	1 / * - / 303	58.0–223.2	[13]
Regional montmorillonite and sepiolite	1 / * - / 298	142.2 and 222.6	[14]
Zeolites and surfactant- zeolites	4 / 6.4 / 298	0.63 and 15.68	[15]
Natural zeolite	6 / 7.5 / 298	19.94	[16]
Mordenite and mordenite nanocrystal	0.25 / 6.5 / 298	30.6 and 46.4	[17]
Microwave rapid synthesized zeolite NaA	1 / 7 / 303	64.8	[18]
Silica nanosheets (vermiculite)	2.3 / 7 / 293	12.66	[19]
PAAm/DxS hydrogels	0.67 / 5.5 / 298	20.22	[24]
HA-Am-PAAm-B	2 / 6.0 / 303	242.4	[33]
NSC-*g*-PAAm/APT	4 / 6.0 / 303	135.14	[35]

*Not available; **Values obtained with reference to bare montmorillonite or clinoptilolite content of the composite (see Section 2.1)

which revealed that the doses were 1.4 and 7.1 g L^{-1} for PAAm-Z and PAAm-Mt, respectively. The lower amount found for PAAm-Z should be evidence for the cost effectiveness of this composite.

With reference to the DR model, $8 < E_{DR} < 20$ kJ mol^{-1} is assumed to be the energy range defining the adsorption process is chemical via ion exchange and/or complex formation under the influence of Coulomb forces.[41] The E_{DR} values were 18.8 kJ mol^{-1} for PAAm-Z and 12.2 kJ mol^{-1} for PAAm-Mt.

2.2. Temperature effect on adsorption and thermodynamic parameters

Thermodynamics of the adsorption was elucidated by the changes in distribution coefficients ($K_d = Q/C_e$) with temperature. The slopes ($\Delta H/R$) and intercepts ($\Delta S/R$) of the depiction of '$\ln K_d$' vs. 1/T (Figure 5) provided adsorption enthalpy and entropy with reference to

$$\ln K_d = \Delta S/R - \Delta H/RT \tag{9}$$

and ΔG values for 298 K were then calculated from the Van t'Hoff equation:

$$\Delta G = \Delta H - T\Delta S \tag{10}$$

The enthalpy and entropy changes were $\Delta H > 0$ and $\Delta S > 0$ for MB adsorption onto both composites (Table 3), implying that the overall process was endothermic and the randomness throughout the adsorption process increased. Gibbs free enthalpy change was $\Delta G < 0$, i.e. the adsorption process was spontaneous. For MB adsorption, the tendency of these magnitudes was concordant with those found by Ghosh and Bhattacharyya[8] for kaolinite ($\Delta H = 13.5$ kJ mol^{-1}, $\Delta S = 88.2$ J mol^{-1}, and $\Delta G = -13.8$ kJ mol^{-1}), by Weng and Pan[11] for spent activated clay ($\Delta H = 12.2$ kJ mol^{-1}, $\Delta S = 153.4$ J mol^{-1}, and $\Delta G = -34.0$ kJ mol^{-1}) and by Han et al.[16] for a natural zeolite ($\Delta H = 12.9$ kJ mol^{-1}, $\Delta S = 75.8$ J mol^{-1}, and $\Delta G = -11.3$ kJ mol^{-1}). Beside these,

exothermic adsorption was reported by Anirudhan and Tharun[25] for MB^+ adsorption onto polymethacrylic acid grafted cellulose/bentonite composite (ΔH = –2.43 kJ mol^{-1}, ΔS = 10.8 J mol^{-1}, and ΔG = –5.66 kJ mol^{-1}).

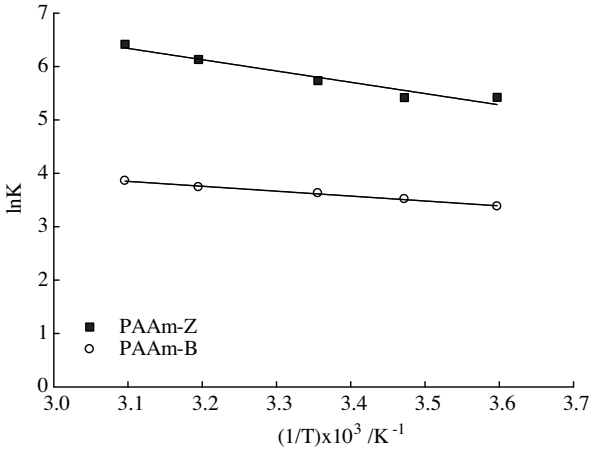

Figure 5. Temperature dependence of adsorption.

Table 3. Thermodynamic parameters for adsorption of MB onto PAAm-Mt and PAAm-Z.

	ΔH/kJ mol^{-1}	ΔS/J mol^{-1} K^{-1}	–ΔG/kJ mol^{-1}	R^2
PAAm-Z	17.6	107.2	14.4	0.943
PAAm-Mt	7.6	55.7	9.0	0.994

The findings of the present study are seemingly contrary to the adsorption phenomenon; the expected changes in entropy are negative since the molecules adsorbed onto the adsorbent are in more regular state than their state in the solution system. Furthermore, the adsorption process represents an energetically more stable situation, i.e. the enthalpy change is also expected to be negative. However, experimental determination of such values is only possible for solid (adsorbent)–gas (adsorbate) systems. As implied by Ghosh and Bhattacharyya,[8] the determination of entropy and enthalpy changes specifically for the adsorbate–adsorbent system in a solution is almost impossible due to the involvement of multicoactions out of the system alone, e.g., solvent–adsorbent, solvent–adsorbate, and dissociative coactions. Eventually, as reported here, the values determined in such studies represent the magnitude of changes in thermodynamic quantities throughout the whole process in the adsorption environment.

2.3. Effect of contact time

The kinetics of MB adsorption onto PAAm-Mt and PAAm-Z were investigated in view of dependence on MB concentration (200 and 500 mg L^{-1} MB) and temperature (293 and 313 K) for both composites; however, the results obtained for PAAm-Mt did not yield any significantly different results under the studied conditions. Thus, Table 4 contains only one set of results for PAAm-Mt. The compatibility of the time dependence of adsorption to pseudo-first and -second order kinetics, and Weber–Morris models (Eqs. (11)–(13)) is presented in Figures 6 and 7.

$$\text{Pseudo-first order model } Q_t = Q_e(1 - e_1^{-kt}) \tag{11}$$

$$\text{Pseudo-second order model } (t/Q_t) = (1/k_2 Q_e^2) + (t/Q_e) \tag{12}$$

$$\text{Weber–Morris model } Q_t = k_{w1,2} t^{0.5}, \tag{13}$$

Table 4. Kinetic parameters for MB adsorption onto PAAm-Z and PAAm-Mt.

	PAAm-Mt			
Kinetic models	C_0 = 200 mg L^{-1}	C_0 = 200 mg L^{-1}	C_0 = 500 mg L^{-1}	
Pseudo-first order	293 K	293 K	293 K	313 K
k_1 / min^{-1}	0.14	5.43	7.86	9.19
Q_{mod} / mol kg^{-1}	0.014	0.053	0.14	0.14
Q_e / mol kg^{-1}	0.014	0.056	0.14	0.14
$H_1 \times 10^3$ / mol kg^{-1} min^{-1}	1.97	2.88	1.06	1.26
R^2	0.955	0.753	0.928	0.951
Pseudo-second order				
k_2 / mol^{-1} kg min^{-1}	11.5	1.18	0.82	1.05
Q_{mod} / mol kg^{-1}	0.015	0.061	0.15	0.15
Q_e / mol kg^{-1}	0.014	0.056	0.14	0.14
$H_2 \times 10^3$ / mol kg^{-1} min^{-1}	2.25	3.70	16.0	20.6
R^2	0.999	0.992	0.999	0.999
Weber–Morris model				
$k_{w1} \times 10^3$ / mol kg^{-1} $min^{0.5}$	2.67	4.34	14.1	20.5
R^2	0.955	0.979	0.937	0.985
$k_{w2} \times 10^3$ / mol kg^{-1} $min^{0.5}$	0.20	0.49	1.14	1.08
R^2	0.940	0.945	0.863	0.848

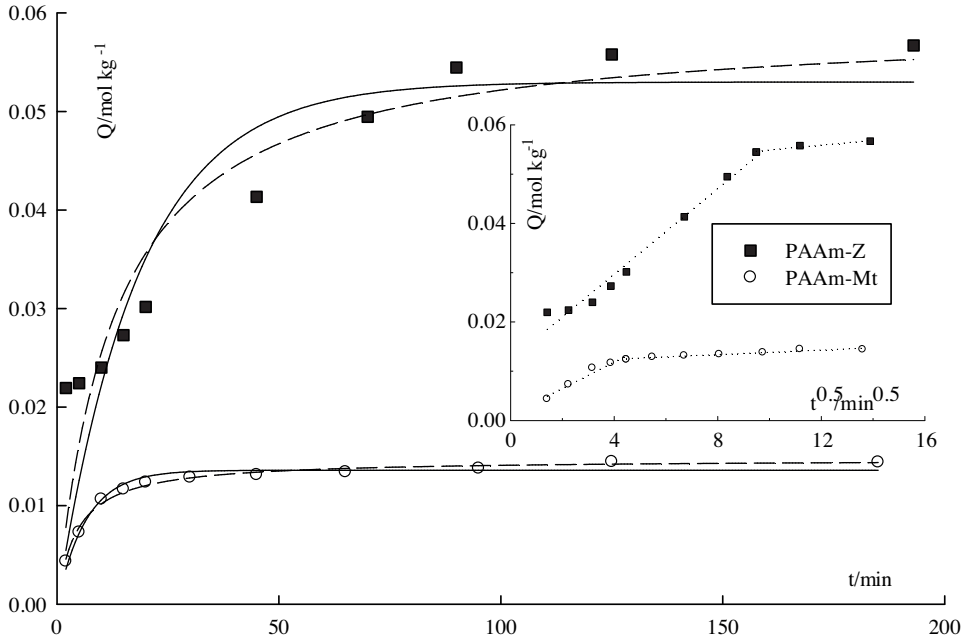

Figure 6. Compatibility of MB adsorption kinetics to pseudo-first order (solid line), pseudo-second order (dashed line), and Weber–Morris models (inset).

where Q_t and Q_e are the adsorbed amounts (mol kg^{-1}) at time t and equilibrium, respectively; and k_1 (min^{-1}), k_2 (kg mol^{-1} min^{-1}), and k_w (mol kg^{-1} $min^{-1/2}$) are the pseudo-first and -second order, and Weber–Morris rate constants, respectively. Initial adsorption rate (H) was calculated from Eq. (14).[42]

$$H_1 = k_1 Q_e \text{ and } H_2 = k_2 Q_e^2 \tag{14}$$

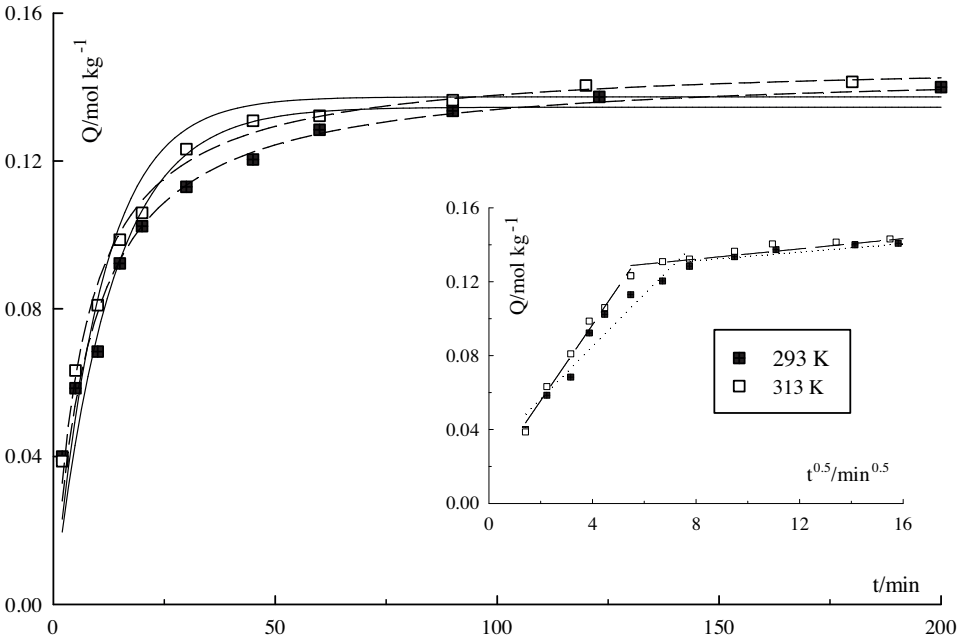

Figure 7. Fitting the time dependence of MB adsorption onto PAAm-Z at 293 and 313 K to pseudo-first order (solid line), pseudo-second order (dashed line), and Weber–Morris models (inset).

The coefficients of regression proved that the adsorption kinetics was best described by the second order model despite the fact that the fitting to the first order model was also significant ($P < 0.05$). Contrary to the rate constants, the sequence of initial adsorption rate (H_2) derived from the second order model was PAAm-Z > PAAm-Mt.

The MB adsorption onto PAAm-Z was energetically evaluated to find out the adsorption activation energy and enthalpy (E_A and ΔH_A) by using Arrhenius equations.[43]

$$\ln(k_{T2}/k_{T1}) = -E_A/R[1/T_2 - 1/T_1] \text{ and } \Delta H_A = E_A - RT \tag{15}$$

As expected, the increasing temperature increased the adsorption constant ($k_{313K} > k_{298K}$), from which the calculated values of the adsorption activation energy (E_a) and enthalpy (ΔH_a) were calculated as 9.4 kJ mol^{-1} and 7.0 kJ mol^{-1}, respectively. The overall process was endothermic ($\Delta H_a > 0$). Adsorption activation energy had a low value, indicating that the MB adsorption was controlled by the combination of chemical and physical (liquid film diffusion) processes.[44] This was also consistent with the suggestions of the compatibility of the data to the Weber–Morris model, providing two linear parts: one with a steep rise and the other with a low gradient providing two rate constants (k_{w1} and k_{w2}). The former is associated with the combination of three physicochemical steps (migration of MB from solution to the surface, diffusion of dye through the boundary layer to the adsorbent surface, and adsorption of dye at the active sites), whereas the latter is the expression

of intraparticle diffusion.[45] The values of k_{w1} significantly higher than those for k_{w2} ($k_{w1} >> k_{w2}$) for both composites were proof the overall adsorption process was governed by the physicochemical interactions on which the contribution of intraparticle diffusion was not considerable.

2.4. Effect of pH

The values of point of zero charge (PZC) represent the pH of the solution where the net surface charge of the material is equal to zero; the surface is positively charged at pH < PZC and is negatively charged at pH > PZC. The PZC values of the composites were obtained for two separate solution environments by the pH measurements at initial and equilibrium: 0.1 M KNO_3 referring to the conventional method[46] and 500 mg L^{-1} MB, besides inspecting the change in MB adsorption with initial pH (see sections 3.2 and 3.3). The PZCs were calculated from the linearity of pH_i vs. the change in difference ($\Delta pH = pH_e - pH_i$), while the data were further considered for pH_i vs. pH_e to figure out the amphoteric features of composites (Figures 8a and 8b).

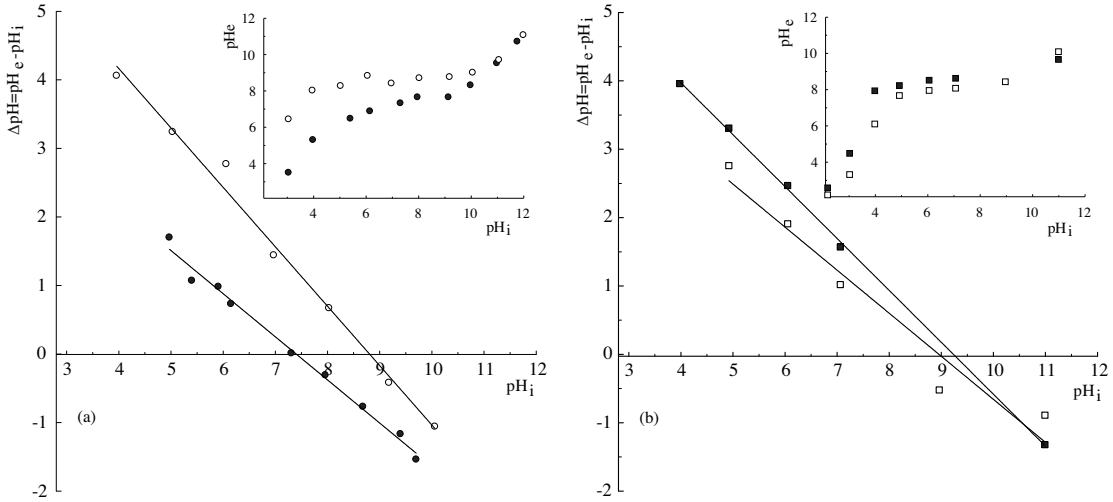

Figure 8. PZC (ΔpH vs. pH_i) and buffering features (pH_e vs. pH_i, as inset) of the composites determined in 0.1 M KNO_3 (a) [PZC = 7.4 (R^2 = 0.991) and 8.8 (R^2 = 0.991) for PAAm-Z and PAAm-Mt] and in 500 mg L^{-1} MB (b) [PZC = 9.2 (R^2 = 0.999) and 8.9 (R^2 = 0.948) for PAAm-Z and PAAm-Mt].

The PZC values were 7.4 and 9.2 for PAAm-Z and 8.8 and 8.9 for PAAm-Mt in the KNO_3 and MB solutions, respectively. This specified that the threshold pH of proton attraction (basicity) was shifted from pH 7.4 to pH 9.2 for PAAm-Z in MB, while there was no difference between the values determined for PAAm-Mt in both media. As illustrated in the insets, both composites had amphoteric features within the range of pH_i 5–10, which buffered the solution environment to about neutral pH (pH_e 6–8).

The changes in MB adsorption with initial pH were not significant (Figure 9) such that the values of mean adsorption ± SEM were 0.021 ± 0.001 mol kg^{-1} (range = 0.016–0.023) for PAAm-Mt and 0.15 ± 0.0005 mol kg^{-1} (range = 0.14–0.15) for PAAm-Z. These results agreed with those reported in previous publications for montmorillonite and sepiolite[14] and natural zeolite[16] (the adsorbed amounts were constant at about 160 and 190 mg g^{-1} for montmorillonite and sepiolite, respectively, and 5 mg g^{-1} for zeolite at initial pH of 2–10). However, some reports indicate that adsorption increased with increasing pH, e.g., for clay[11,13] (from 60% to 95% at pH range from 2.0 to 6.5 and nearly constant at pH values up to 10), for silica nanosheets[19] (from 7.5

to 9.5 mg g^{-1} with increasing pH from 4.0 to 7.0), and for zeolite[15] (from 5 to 6.1 mg g^{-1} with increasing pH from 4 to 9), attributed to the negative charge increase on the surface of adsorbents with rising pH. On the other hand, the decrease at pH $>$ 9 for clay-Na was ascribed to the variations in dimer/monomer-MB formations with pH changes.[47]

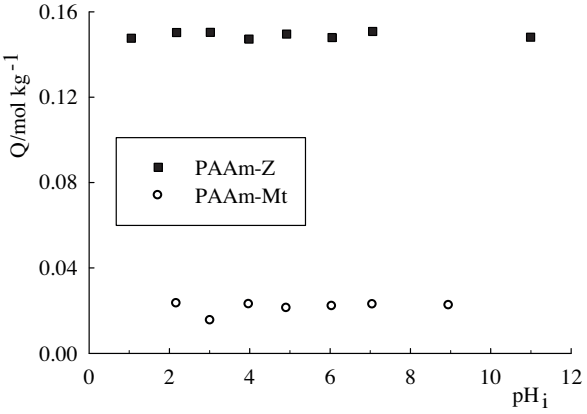

Figure 9. The effect of initial pH on MB adsorption.

By considering the combination of the values of PZC and pH effect on MB adsorption studies, the following mechanisms could be envisaged (M is Si and/or Al, MB^+ is the dye) for which the readers may additionally refer to studies elucidating the adsorption mechanism by ion exchange between H^+ on the surface and MB^+ ions and/or complex formation between MB^+ and negatively charged centers on the adsorbent surface.[11,15,19,28]

1. Mechanisms (1) and (2) should be the explanation of pH shifts and amphoteric properties observed in the PZC investigations,

$$\equiv M-OH+H^+ \leftrightarrow \equiv M-OH_2^+ \text{ at acidic } pH_i (pH_e > pH_i, \Delta pH > 0, pH_e 6-8) \quad (1)$$

$$\equiv M-OH+OH^- \leftrightarrow \equiv M-O^- \text{ at basic } pH_i (pH_e < pH_i, \Delta pH < 0, pH_e 6-8) \quad (2)$$

2. The driving force of dye adsorption should be Coulomb (electrostatic) attractions (mechanisms (3)-(5)) and/or ion exchange resulting in complex formation:

$$\equiv M-OH+MB^+ \leftrightarrow \equiv M-OH:....MB^+ at pH_i = PZC \quad (3)$$

$$\equiv M-OH_2^+ + MB^+ \leftrightarrow \equiv M-OH:....MB^+ + H^+ \text{ at } pH_i < PZC \quad (4)$$

$$\equiv M-O^- + MB^+ \leftrightarrow \equiv M-O^-MB^+ \text{ at basic } pH_i \text{ and } pH_i > PZC \quad (5)$$

(Mechanisms (3) and (5) might also be possible at any pH because of the presence of such available centers).

3. A covalent bonding of MB^+ with aluminosilicate surface (mechanism (6)) might also be proposed as suggested by Wang and Li.[48]

$$\equiv M-OH+H^+ + MB^+ \leftrightarrow \equiv M-MB+H_2O \quad (6)$$

The comparison of FT-IR spectra taken before and after MB adsorption (Figure 10) indicated that the whole pattern of pure composites significantly diminished after MB adsorption but did not lead to a change in any specific peaks related to the functional groups.

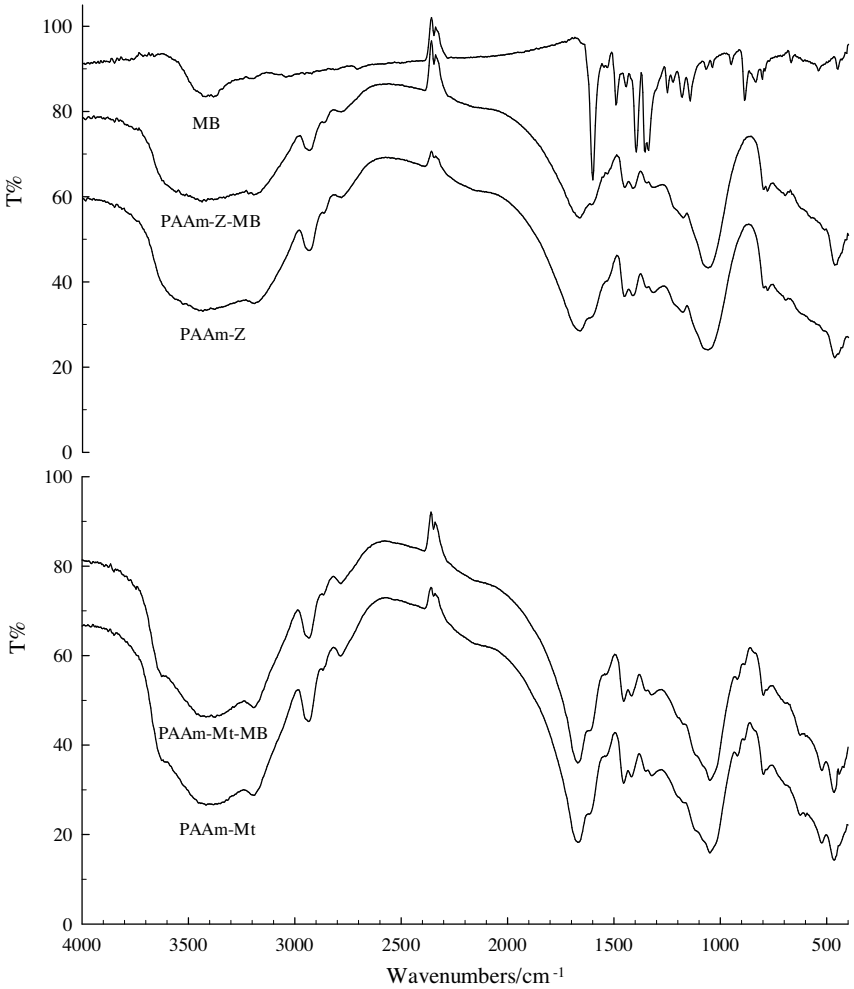

Figure 10. FT-IR patterns of MB and the composites before and after MB adsorption; the spectra had exactly 2 mg of composites in 100-mg KBr pellets with or without MB [The peaks of MB at 1620 cm^{-1} for C=N and C=O, the four peaks appeared between 1250 and 1450 cm^{-1} for aromatic rings, broad bands at 2250 cm^{-1} and 3450 cm^{-1} for S = C=N and N–H respectively.[48,49] The broad appearances at 3500 cm^{-1} in PAAm-Mt/Z spectra were of O–H stretches, the counters within the range of 1000–1700 cm^{-1} and 400–700 cm^{-1} were of silicates in B/Z. The stretches at 3200 and 1700 cm^{-1} of C=O of amide and 2900 cm^{-1} of C–H were of PAAm of PAAm-Mt/Z.[29]

This suggested that the interaction between MB molecules and aluminosilicate surface had high complexity. Although $\equiv$ M – OH groups and positively charged auxochromes (N and/or S, see MB scheme) were expected to be the key components of adsorption,[3] their same FT-IR profiles should be evidence the chromophores (π-electrons) of MB and H-bonds also took part in the adsorption mechanism. Due to these multiinteractions, the adsorbed MB molecules strongly bond to the composite surface.

In conclusion, the adsorptive features of aluminosilicates (montmorillonite and clinoptilolite) entrapped in PAAm for other complex organic compounds like MB were investigated. The composites (especially PAAm-

Z) had considerably high adsorption capacities in comparison to previously reported aluminosilicate-based adsorbents. The adsorption was endothermic ($\Delta H > 0$) and the randomness at the solid–solution interface increased ($\Delta S > 0$) throughout the adsorption process. The value of free adsorption enthalpy ($\Delta G < 0$) was the indication of spontaneity. The adsorption kinetics could be explained by the pseudo-second order model and the adsorption was controlled by the combination of chemical and physical (liquid film diffusion) processes in which the contribution of intraparticle diffusion was not significant. This was consistent with the low value of the adsorption activation energy. The composites had amphoteric features buffering the adsorption environment to about neutral pH. Thus MB adsorption was not pH dependent. The driving force of adsorption was envisaged to be Coulomb (electrostatic) attractions and/or ion exchange resulting in complex formation. Overall, the application of zeolite as a naturally occurring aluminosilicate could be considered an economical alternative to the current adsorbents.

3. Experimental

3.1. Reagents

Na-montmorillonite in 98% purity was purchased from Sigma (USA). Clinoptilolite was obtained from Central North Anatolian occurrences associated with Eocene submarine volcanism. The certified (IMO GmbH) clinoptilolite composition was 71.89% SiO_2, 15.16% Al_2O_3, 6.51% CaO, 1.80% Fe_2O_3, 1.80% MgO, 1.06% Na_2O, and 0.59% SrO. The mineral is composed of ~90% clinoptilolite, as clinoptilolite $\{(Na,K)_6 \cdot [Al_6Si_{30}O_{72}] \cdot 24H_2O\}$ and mordenite $\{Na_3KCa_2 \cdot [Al_8Si_{40}O_{96}] \cdot 28H_2O\}$, 5% quartz, 5% feldspar, and smectite in trace level. The ratio of SiO_2/Al_2O_3 is 4.7, suggesting that the mineral is clinoptilolite with reference to the classification of the International Mineralogical Association.[53]

N,N′-methylene-bisacrylamide and N,N,N′,N′-tetramethylethylenediamine (TEMED) were purchased from Sigma. Acrylamide (AAm) monomer, ammonium peroxodisulfate (APS), and MB were obtained from Merck. Distilled water was used throughout the investigation.

3.2. Preparation of PAAm-Mt and PAAm-Z composites

PAAm-B and PAAm-Z was prepared by direct polymerization of AAm monomer in dispersions of Mt and Z to achieve 2:1 mass ratio of PAAm to the mineral. APS and TEMED as the initiator and propagator of the polymerization, and N,N'-methylene-bisacrylamide as cross linking agent were used. The obtained composite gels were washed with distilled water until effluent attained water conductivity, dried at ambient temperature, ground, and sieved to an average particle size of 50 mesh.[54]

The composites were characterized by FT-IR spectra (Unicam, Mattson-1000), XRD (Rigaku Ultima-IV), and SEM views (JEOL/JSM-6335F). The cation exchange capacity (CEC) of Mt, Z, and the composites was determined by ammonium acetate method[55] where the colorimetric technique was used for ammonium measurements.[56] Point of zero charge (PZC) of the composites was determined for two different solution environments: in the presence of 0.1 M KNO_3 as an inert electrolyte[46] and in the presence of MB, while testing the adsorption dependence on initial pH (see section 3.3).

3.3. MB uptake studies

Batch experiments were conducted to investigate the effect of initial MB concentration, contact time, temperature, and pH on adsorption. Certain fractions of the composites (0.1 g) were interacted with 10 mL of dye

solution in Pyrex tubes and the mixtures stirred on a plate shaker. Conventionally, the solution–composite contact time was 24 h unless stated otherwise. The equilibrium solutions were separated by centrifugation for 5 min at 2000 rpm. MB concentrations in 200-μL duplicates of supernatants were determined by absorbance measurement (Shimadzu-160A spectrophotometer) at 665 nm.

For the investigation of initial MB concentration on adsorption, the adsorbents were equilibrated with solutions containing 25–2000 mg L^{-1} MB at pH 4.0–6.5 as obtained from the dissolution of MB salt. The temperature effect on dye removal was determined at 278, 288, 298, 313, and 323 K. The effects of initial MB concentrations and temperature on the adsorption kinetics were investigated for 200 and 500 mg L^{-1} dye concentrations at 293 and 313 K. While 20 mL of MB solutions was interacting with 0.20 g of composites, 200 μL of solution fraction was taken at predetermined time intervals up to 200 min (sufficient time to attain equilibrium).

The effect of initial pH on adsorption was also tested; 0.1 g of the composites was added to MB solutions ($[MB]_0$ = 500 mg L^{-1}) after pHs were adjusted to 1.0–11.0 by addition of 0.1 mol L^{-1} NaOH or HCl and final pHs were recorded after 24 h equilibration (A Thermo, Orion 420 A+ pH meter).

Acknowledgment

This work was supported by the Research Fund of Cumhuriyet University (CÜBAP).

References

1. Batzias, F. A.; Sidiras, D. K. *J. Hazard. Mater.* **2007**, *141*, 668–679.
2. Tsai, F. C.; Ma, N.; Tsai, L. C.; Shu, C. M.; Jiang, T.; Chang, H. C.; Wen, S.; Zhang, C.; Chiang, T. C.; Chu, Y. C.; et al. In *Syntheses and Applications of Carbon Nanotubes and Their Composites*; Suzuki, S. Eds. Open Access Book, ISBN 978-953-51-1125-2, 2013, pp. 467–478.
3. Gupta, V. K.; Suhas. *J. Environ. Manag.* **2009**, *90*, 2313–2342.
4. Gupta, V. K.; Pathania, D.; Agarwal, S.; Sharma, S. *J. Mol. Liq.* **2012**, *174*, 86–94.
5. Chandrasekhar, S.; Pramada, P. N. *Adsorption* **2006**, *12*, 27–43.
6. Kiernan, J. A. *Biotech. Histochem.* **2001**, *76*, 261–277.
7. Rafatullah, V.; Sulaiman, O.; Hashim, R.; Ahmad, A. *J. Hazard. Mater.* **2010**, *177*, 70–80.
8. Ghosh, D.; Bhattacharyya, K. G. *Appl. Clay Science* **2002**, *20*, 295–300.
9. Ismail, B.; Hussain, S. T.; Akram, S. *Chem. Eng. J.* **2013**, *219*, 395–402.
10. Hajjaji, M.; Alami, A.; El Bouadili, A. *J. Hazard. Mater.* **2006**, *B135*, 188–192.
11. Weng, C. H.; Pan, Y. F. *J. Hazard. Mater.* **2007**, *144*, 355–362.
12. Gil, A.; Assis, F. C. C.; Albeniz, S.; Korili, S. A. *Chem. Eng. J.* **2011**, *168*, 1032–1040.
13. Auta, M.; Hameed, B. H. *J. Ind. Eng. Chem.* **2013**, *19*, 1153–1161.
14. Bilgiç, C. *J. Colloid Interface Sci.* **2005**, *281*, 33–38.
15. Jin, X.; Jiang, M.; Shan, X.; Pei, Z.; Chen, Z. *J. Colloid Interface Sci.* **2008**, *328*, 243–247.
16. Han, R.; Zhang, J.; Han, P.; Wang, Y.; Zhao, Z.; Tang, M. *Chem. Eng. J.* **2009**, *145*, 496–504.
17. Sohrabnezhad, Sh.; Pourahmad, A. *Desalination* **2010**, *256*, 84–89.
18. Sapawe, N.; Jalil, A. A.; Triwahyono, S.; Shah, M. I. A.; Jusoh, R.; Salleh, N. F. M.; Hameed, B. H.; Karim, A. H. *Chem. Eng. J.* **2013**, *229*, 388–398.

19. Zhao, M.; Tang, Z.; Liu, P. *J. Hazard. Mater.* **2008**, *158*, 43–51.
20. Acemioğlu, B.; Ertaş, M.; Alma, M. H.; Usta, M. *Turk. J. Chem.* **2014**, *38*, 454–469.
21. Ma, C.; Cao, L.; Wang, X.; Zhang, L.; Shi, M.; Wang, J. *J. Supercrit. Fluids* **2012**, *62*, 232–239.
22. Al, E.; Güçlü, G.; Iyim, T. B.; Emik, S.; Özgümüş, S. *J. Appl. Polym. Sci.* **2008**, *109*, 16–22.
23. Wang, L.; Zhang, J.; Wang, A. *Colloids Surf., A* **2008**, *322*, 47–53.
24. Perju, M. M.; Dinu, M. V.; Dragan, E. S. *Sep. Sci. Technol.* **2012**, *47*, 1322–1333.
25. Anirudhan, T. S.; Tharun, A. R. *Chem. Eng. J.* **2012**, *181–182*, 761–769.
26. Meral, K.; Metin, Ö. *Turk. J. Chem.* **2014**, *38*, 775–782
27. Baybaş, D.; Ulusoy, U. *Appl. Clay Sci.* **2011**, *51*, 138–146.
28. Rahchamani, J.; Mousavi, H. Z.; Behzad, M. *Desalination* **2011**, *267*, 256–260.
29. Ulusoy, U.; Şimşek, S. *J. Hazard. Mater. B* **2005**, *127*, 163–171.
30. Şenol, Z. M.; Ulusoy, U. *Chem. Eng. J.* **2010**, *162*, 97–105.
31. Baybaş, D.; Ulusoy, U. *J. Hazard. Mater.* **2011**, *187*, 241–249.
32. Yi, J. Z.; Zhang, L. M. *Bioresour. Technol.* **2008**, *99*, 2182–2186.
33. Anirudhan, T. S.; Suchithra, P. S.; Radhakrishnan, P. G. *Appl. Clay Sci.* **2009**, *43*, 336–342.
34. Bajpai, S. K.; Shrivastava, S. *J. Appl. Polym. Sci.* **2011**, *119*, 2525–2532.
35. Li, Q.; Zhao, Y.; Wang, L.; Aiqin, W. *Korean J. Chem. Eng.* **2011**, *28*, 1658–1664.
36. Qiu, H.; Qiu, Z.; Wang, J.; Zhang, R.; Zheng, F. *J. Appl. Polym.* **2014**, *131*, 1–9.
37. Sing, K. S. W. *Pure Appl. Chem.* **1982**, *54*, 2201–2218.
38. Doula, M. K. Chemosphere **2007**, *67*, 731–740.
39. Alexandre, M.; Dubois, P. *Mater. Sci. Eng.* **2000**, *28*, 1–63.
40. McKay, G.; Poots, V. J. P. *J. Chem. Technol. Biotechnol.* **1980**, *30*, 279–292.
41. Baybaş, D.; Ulusoy, U. *J. Solid State Chem.* **2012**, *194*, 1–8.
42. Ho, Y. S.; McKay, G. *Process Biochemistry* **1999**, *34*, 451–465.
43. Winzor, D. J.; Jackson, C. M. *J. Mol. Recognit.* **2006**, *19*, 389–407.
44. Shuchuan, P.; Shisheng, W.; Tianhu, C.; Shaotong, J.; Chuanhu, H. *Acta Geol. Sin.* **2006**, *80*, 236–242.
45. Kannan, N.; Sundaram, M.M. *Dyes Pgm.* **2001**, *51*, 25–40.
46. Mullet, M.; Fievet, P.; Szymczyk, A.; Foissy, A.; Reggiani, J. C.; Pagetti, J. *Desalination* **1999**, *121*, 41–48.
47. Elaziouti, A.; Laouedj, N.; Ahmed, B. *J. Chem. Eng. Process Technol.* **2011**, *2*, 2–5.
48. Wang, S.; Li, H. *Microporous Mesoporous Mater.* **2006**, *97*, 21–26.
49. vander Maas, J.H. *Basic Infrared Spectroscopy*; Second Edition, Heyden and Son Ltd.: London, UK, 1972 .
50. Hasnat, M. A.; Safwan, J. A.; Islam, M. S.; Rahman, Z.; Karim, M. R.; Pirzada, T. J.; Samed, A. J.; Rahman, M. M. *J. Ind. Eng. Chem.* **2015**, *21*, 787–791.
51. Boiarkina, I.; Pedron, S.; Patterson, D. A. *Appl. Catal. B* **2011**, *110*, 14–24.
52. Attarchi, N.; Montazer, M.; Toliyat, T. *Appl. Catal. A* **2013**, *467*, 107–116.
53. Godelitsas, Ath.; Armbruster, Th. *Micropor. Mesopor. Mat.* **2003**, *61*, 3–24.
54. Ulusoy, U.; Şimşek, S.; Ceyhan, Ö. *Adsorption* **2003**, *9*, 165–175.
55. Ross, D. S. In *Recommended Soil Testing Procedures for the Northeastern United States*; Sims, J.T.; Wolf, A., Eds. Northeast Regional Bulletin #493. Agricultural Experiment Station, University of Delaware, Newark, DE, USA, 1995, pp. 62–69.
56. Chaney, A. L.; Marbachch, E. P. *Clin. Chem.* **1962**, *8*, 130–132.